EasyChair Preprint

№ 4444

Generalized Orthogonal Moment

Yijian Zhang, Zhou Yuan and Jianwei Yang

October 20, 2020

Generalized orthogonal moment

Yijian Zhang
Reading Academy，
Nanjing University of Information Science and Technology, Nanjing China
e-mail:bm803049@student.reading.ac.uk

Zhou Yuan, and Jianwei Yang
School of Mathematics & Statistics,
Nanjing University of Information Science and Technology, Nanjing China
e-mail: yjianw@nuist.edu.cn

Abstract: **Orthogonal moments play an important role in image analysis *d*ue to their ability to represent images with minimum amount of information redundancy and high level of noise robustness. Recently, several fractional-order orthogonal moments have been proposed. But functions used for the construction of these moments are restricted to fractional-order polynomials. In this paper, orthogonal moments are further generalized to *generalized orthogonal moments* (GOMs). A general framework is proposed for the construction of functions used in GOMs. Orthogonal polynomials used in traditional orthogonal moments and fractional-order polynomials used in fractional-order orthogonal moments are all special cases of the proposed framework. Properties of the proposed GOMs have been proven. New set of orthogonal moments have also been constructed by choosing several particular functions. Experimental results show the superiority of these moments.**

Keywords：fractional-order orthogonal moment; generalized orthogonal moment (GOM); image reconstruction; rotation invariance; robustness to noise.

I. INTRODUCTION

As the global invariant descriptors, moment have been widely studied[1,2,3,4] and effectively applied in various fields, such as pattern recognition[5], image reconstruction[6], edge detection[7] and water marking[8], etc. They can be roughly divided into non-orthogonal moments and orthogonal moments. Non-orthogonal moments are usually invariant to scaling, rotation and translation, but they are highly sensitive to noise and with information redundancy. Furthermore, the image can hardly be reconstructed from non-orthogonal moments. In contrast, orthogonal moments have been shown to be more robust to noise and are of little information redundancy. Consequently, image can be easily reconstructed by orthogonal moments.

During the latest years, the study of orthogonal moments with fractional-order have received much attention. In terms of fractional-order shifted Legendre polynomials and fractional-order radial shifted Legendre polynomials, Xiao et.al [9] define two types of fractional-order orthogonal moments in Cartesian coordinate and polar coordinate respectively. Using the so-called fractional-order Fourier-Mellin polynomials, Zhang et.al[10] propose fractional-order orthogonal Fourier-Mellin moments. Benouini et.al [11] introduce a new type of fractional-order orthogonal moments, called Fractional-order Chebyshev moments. Recently, Chen et.al [12] extend the Zernike moments to the quaternion and fractional-order framework for the features extraction of color image. However, all of these constructions are based on the generalization of integer-order polynomials to real-order polynomials. In fact, these constructions can be further generalized.

In this paper, *generalized orthogonal moments* (GOMs) are proposed. It sets up a general framework for the construction of orthogonal moments. Radial basis functions other than integer-order polynomials and fractional-order polynomials can be employed to construct orthogonal moments. We take the construction of the *generalized Legendre moments* (GLMs) as an example. Orthogonality and rotation invariance of these moments have been proven. Several functions are employed to construct new set of orthogonal moments. Several experiments have been conducted to show the performance of these constructed moments.

Section 2 provides the framework of GOMs and some properties of GOMs are also presented. Section 3 describes some details for the generalized Legendre moments. Experimental results are given in Section 4. Finally, concluding remarks are listed in Section 5.

II. GENERALIZED ORTHOGONAL MOMENT

A. Orthogonal moment

Orthogonal polynomials can be expressed as follows:

$$P_n(x) = \sum_{i=0}^{n} c_{n,i} x^i \tag{1}$$

where n is a non-negative integer, $c_{n,i}$ denotes the coefficient of each monomial.

Let $f(x,y)$ and $f(r,\theta)$ denote the image in Cartesian coordinate and polar coordinate respectively. The $(n+m)$-order orthogonal moment are defined as follows:

$$\begin{aligned} Z_{nm}^{C} &= \int\int_{R^2} P_n(x) P_m(y) f(x,y) dxdy , \\ Z_{nm}^{P} &= \int\int_{R^2} P_n(r) e^{-jm\theta} f(r,\theta) rdrd\ \theta \end{aligned} \tag{2}$$

Here, $P_n(x), P_n(r)$ both satisfy the following conditions:

$$\begin{aligned} \int_0^1 P_n(x) P_m(x) dx &= k_1 \delta_{nm} , \\ \int_0^1 P_n(r) P_m(r) rdr &= k_2 \delta_{nm} \end{aligned} \tag{3}$$

where $k_1, k_2 > 0$ and $\delta_{nm} = \begin{cases} 1, n = m \\ 0, n \neq m \end{cases}$.

B. Generalized orthogonal moment

Choose function $h(x)$ such that its domain and range are both in $(0,1]$. Then, the traditional polynomial P_n can be generalized to the following generalized polynomials:

$$\begin{aligned} \bar{G}P_n(x) &= \sqrt{h'(x)}P_n[h(x)] = \sqrt{h'(x)}\sum_{i=0}^{n} c_{n,i}[h(x)]^i, \\ \hat{G}P_n(r) &= \sqrt{\frac{h'(r)}{r}}P_n[h(r)] = \sqrt{\frac{h'(r)}{r}}\sum_{i=0}^{n} c_{n,i}[h(r)]^i \end{aligned} \tag{4}$$

Here, $h'(x)$ is the derivative function of $h(x)$.

Definition 1

As for non-negative integers n, m,

$$\begin{aligned} GZ_{nm}^{C} &= \int\int_{R^2} \bar{G}P_n(x)\bar{G}P_m(y) f(x,y)dxdy, \\ GZ_{nm}^{P} &= \int\int_{R^2} \hat{GP}_n(r) e^{-jm\theta} f(r,\theta) r dr d\theta \end{aligned} \tag{5}$$

GZ_{nm}^{C}, GZ_{nm}^{P} are called the $(n+m)$ -order *generalized orthogonal moments* (GOMs) of the image in Cartesian and polar coordinates, respectively.

Remark:

1) Fractional-order orthogonal moments are only special cases of GOMs.

If we choose $h(x) = x^{\alpha}, (\alpha > 0)$, it follows that:

$$\begin{aligned} \bar{G}P_n(x) &= \sqrt{\alpha}\sum_{i=0}^{n} c_{n,i} x^{\alpha i + ((\alpha-1)/2)}, \\ \hat{GP}_n(r) &= \sqrt{\alpha}\sum_{i=0}^{n} c_{n,i} r^{\alpha i + ((\alpha-2)/2)} \end{aligned} \tag{6}$$

Fractional-order orthogonal polynomials in Eq.(6) are employed to define the fractional-order orthogonal moment defined in [9].

2) GOMs defined by Eq.(5) are generalized orthogonal moments.

In fact, we can take $h(x)$ as more general functions, such as $h(x) = \sin(\frac{\pi}{2}x^{\alpha}), h(x) = [\sin(\frac{\pi}{2}x^{\alpha})]^2$, etc.

Above all, GOMs defined in this paper is a further generalization of the fractional-order orthogonal moment defined in [9].

C. Properties of GOMs

1) Orthogonality

$\bar{G}P_n(x), \hat{GP}_m(r)$ defined by Eq.(4) both satisfy the following condition:

$$\begin{aligned} \int_0^1 \bar{G}P_n(x)\bar{G}P_m(x)dx &= k_1\delta_{nm}, \\ \int_0^1 \hat{GP}_n(r)\hat{GP}_m(r) r dr &= k_2\delta_{nm} \end{aligned} \tag{7}$$

Proof:

$$\begin{aligned} \int_0^1 \bar{G}P_n(x)\bar{G}P_m(x)dx &= \int_0^1 \sqrt{h'(x)}P_n[h(x)]\sqrt{h'(x)}P_m[h(x)]dx \\ &= \int_0^1 h'(x)P_n[h(x)]P_m[h(x)]dx \\ &= \int_0^1 P_n[h(x)]P_m[h(x)]d[h(x)] \\ &= k_1\delta_{nm} \end{aligned} \tag{8}$$

Similarly, it can be shown that $\int_0^1 \hat{GP}_n(r)\hat{GP}_m(r) r dr = k_2\delta_{nm}$ holds.

Therefore, the image can be reconstructed by using $\bar{G}P_n(x), \hat{GP}_m(r)$ defined above:

$$\begin{aligned} f(x,y) &= \sum_{n=0}^{n_{\max}}\sum_{m=0}^{m_{\max}} GZ_{nm}^{C} GP_n(x) GP_m(y), \\ f(r,\theta) &= \sum_{n=0}^{n_{\max}}\sum_{m=0}^{m_{\max}} GZ_{nm}^{P} GP_n(r) e^{jm\theta} \end{aligned} \tag{9}$$

2) Rotation invariance

Module of GZ_{nm}^{P} is rotation invariant.

Proof:

Suppose that $\tilde{f}(r,\theta)$ is the image rotated by $f(r,\theta)$ with an angle ϕ: $\tilde{f}(r,\theta) = f(r,\theta-\phi)$. Let $\tilde{\theta} = \theta - \phi$, it follows that $\theta = \tilde{\theta} + \phi, d\tilde{\theta} = d\theta$. Then GOMs of $\tilde{f}(r,\theta)$ satisfy the following relation:

$$\begin{aligned} \tilde{GZ}_{nm}^{P} &= \iint_{R^2} \hat{GP}_n(r) e^{-jm\theta} f(r,\theta-\phi) r dr d\theta \\ &= \iint_{R^2} \hat{GP}_n(r) e^{-jm(\tilde{\theta}+\phi)} f(r,\tilde{\theta}) r dr d\tilde{\theta} \\ &= GZ_{nm}^{P} e^{-jm\phi} \end{aligned} \tag{10}$$

Hence, $\left|\tilde{GZ}_{nm}^{P}\right| = \left|GZ_{nm}^{P}\right|$. In other words, GOMs GZ_{nm}^{P} are rotation invariants.

III. Generalized Legendre moment

A. GLM

$P_n(x)$ defined in Eq.(1) can be any polynomial that satisfies the orthogonal condition. We take the classical Legendre moment [13] as an example:

$$L_n(x) = \sum_{i=0}^{n} c_{n,i} x^i = \sum_{i=0}^{n} (-1)^{n+i} \binom{n}{i} \binom{n+i}{i} x^i \tag{11}$$

According to Eq.(4), we can define GLM as follows:

$$\begin{aligned}\overline{G}L_n(x) &= \sqrt{h'(x)}L_n[h(x)] \\ &= \sqrt{h'(x)}\sum_{i=0}^{n}(-1)^{n+i}\binom{n}{i}\binom{n+i}{i}[h(x)]^i, \\ \hat{G}L_n(r) &= \sqrt{\frac{h'(r)}{r}}L_n[h(r)] \\ &= \sqrt{\frac{h'(r)}{r}}\sum_{i=0}^{n}(-1)^{n+i}\binom{n}{i}\binom{n+i}{i}[h(r)]^i\end{aligned} \tag{12}$$

It follows from Eq.(8) that $\overline{G}L_n(x), \hat{G}L_n(r)$ satisfy the following condition:

$$\begin{aligned}\int_0^1 \overline{G}L_n(x)\overline{G}L_m(x)dx &= \frac{1}{2n+1}\delta_{nm}, \\ \int_0^1 \hat{G}L_n(r)\hat{G}L_m(r)rdr &= \frac{1}{2n+1}\delta_{nm}\end{aligned} \tag{13}$$

Definition 2

For $\overline{G}L_n(x)$ and $\hat{G}L_n(r)$, GLM_{nm}^{C} and GLM_{nm}^{P} are defined as follows:

$$\begin{aligned}GLM_{nm}^{C} &= (2n+1)(2m+1)\int_0^1\int_0^1 \overline{G}L_n(x)\overline{G}L_m(y)f(x,y)dxdy, \\ GLM_{nm}^{P} &= \frac{2n+1}{2\pi}\int_0^1\int_0^{2\pi}\hat{G}L_n(r)e^{-jm\theta}f(r,\theta)rdrd\theta.\end{aligned} \tag{14}$$

GLM_{nm}^{C}, GLM_{nm}^{P} are called the $(n+m)$ -order *generalized Legendre moments* (GLMs) of the image in Cartesian and polar coordinates, respectively.

It is obvious that $\left|GLM_{nm}^{P}\right|$ is rotation invariant. In addition, the images $f(x,y)$, $f(r,\theta)$ can be reconstructed based on GLMs:

$$\begin{aligned}f(x,y) &= \sum_{n=0}^{n_{\max}}\sum_{m=0}^{m_{\max}}GLM_{nm}^{C}\overline{G}L_n(x)\overline{G}L_m(y), \\ f(r,\theta) &= \sum_{n=0}^{n_{\max}}\sum_{m=0}^{m_{\max}}GLM_{nm}^{P}\hat{G}L_n(r)e^{jm\theta}\end{aligned} \tag{15}$$

B. Recursive scheme for fast computation

According to Eq. (12), $\overline{G}L_n(x)$ and $\hat{G}L_n(r)$ satisfy the following recurrence relation [14]:

$$\begin{aligned}\overline{G}L_{n+1}(x) &= \frac{2n+1}{n+1}[2h(x)-1]\overline{G}L_n(x) - \frac{n}{n+1}\overline{G}L_{n-1}(x), \\ \hat{G}L_{n+1}(r) &= \frac{2n+1}{n+1}[2h(r)-1]\hat{G}L_n(r) - \frac{n}{n+1}\hat{G}L_{n-1}(r) \qquad n \ge 1.\end{aligned} \tag{16}$$

For $n = 0, 1$, it follows from Eq.(16) that:

$$\begin{aligned}&\overline{G}L_0(x) = \sqrt{h'(x)}, \quad \overline{G}L_1(x) = \sqrt{h'(x)}[2h(x)-1], \\ &\hat{G}L_0(r) = \sqrt{\frac{h'(r)}{r}}, \quad \hat{G}L_1(r) = \sqrt{\frac{h'(r)}{r}}[2h(r)-1].\end{aligned} \tag{17}$$

The above relation helps us reduce the computation of GLM.

C. Zeros of the generalized Legendre polynomials

It is shown in [15] that the effect of image reconstruction is determined by the number of zeros associated with the polynomials. We take $\overline{G}L_n(x)$ as an example, the reconstruction performance of the image becomes better as the number of zeros of $\overline{G}L_n(x)$ is greater.

Fig.1 shows images of $\overline{G}L_n(x)$ when $n = 1,2,\cdots,10$ with different $h(x)$. For $h(x) = x^{\alpha}, (\alpha > 0)$, we get the fractional-order orthogonal moment. It is obvious that $\overline{G}L_n(x)$ has n zeros.

As for GOMs, if we choose $h(x) = \sin(\frac{\pi}{2}x^2)$ or $h(x) = [\sin(\frac{\pi}{2}x)]^2$, $\overline{G}L_n(x)$ has $n+2$ zeros.

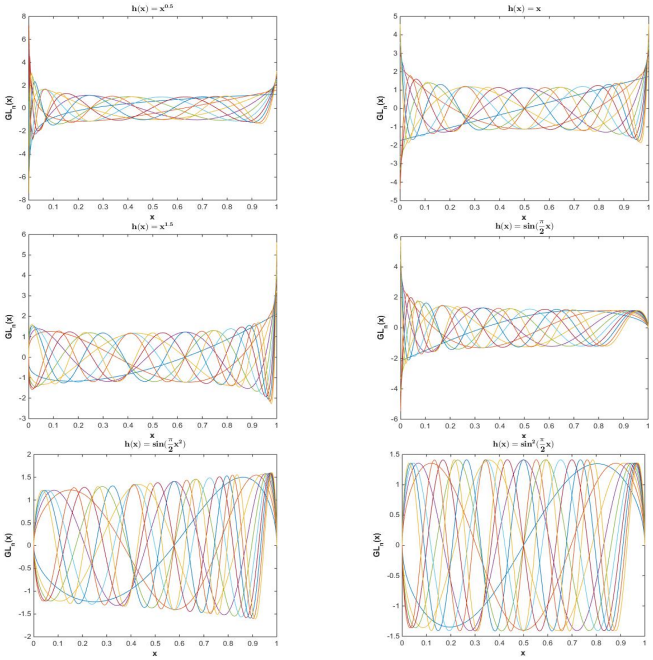

Fig.1 $\overline{G}L_n(x)$ with different $h(x)$

IV. EXPERIMENTS RESULTS

The purpose of the following experiments is to test the reconstitution performance, rotation invariance and robustness to noise of GOMs. Take GLM as an example. The test objectives are 30 Chinese character in Fig.2(a) and Coil-20 images in Fig.2(b). These images are of size 128×128.

The following functions are employed in the construction of GOMs

$h(x) = x^{\alpha}(\alpha = 0.5,\ 1,\ 1.5)$, $h(x) = \sin(\frac{\pi}{2}x)$,

$h(x) = \sin(\frac{\pi}{2}x^2)$, $h(x) = [\sin(\frac{\pi}{2}x)]^2$

If $\alpha = 1$, GLMs constructed by $h(x) = x^{\alpha}$ is the traditional orthogonal moment. As for $\alpha = 0.5,\ 1.5$, GLMs is the fractional-order orthogonal moment. The latter three cases are the GOMs used in this paper.

(a) 30 Chinese characters

(b) Coil-20 image database

Fig.2 Test objectives

A. *Image reconstruction*

The following *mean square error* (MSE) is employed to measure the effect of the reconstruction with the GLMs in Cartesian coordinate system.

$$MSE = \frac{\sum_{x}\sum_{y}\left[f(x,y) - \bar{f}(x,y)\right]^2}{\sum_{x}\sum_{y} f(x,y)^2} \tag{18}$$

Here, $f(x,y)$ denotes the original image, $\bar{f}(x,y)$ denotes the reconstructed image. Fig.3 shows the test result of the first image in Coil-20 database by using GLM_{nm}^{C} to reconstruct image and taking values of $n_{\max} = m_{\max} = 5, 10, 15, 20$, respectively.

According to Fig.3, it is observed that the reconstruction error of GLMs is lower than those of the traditional and fractional-order orthogonal moment when $h(x) = \sin(\frac{\pi}{2}x)、\sin(\frac{\pi}{2}x^2)、[\sin(\frac{\pi}{2}x)]^2$. In particular, the reconstruction performance of $h(x) = [\sin(\frac{\pi}{2}x)]^2$ is the best.

Further, we use GLM_{nm}^{C} to reconstruct image by adopting images in Fig.2(a), Fig.2(b) as test objectives and taking $n_{\max} = m_{\max} = 10, 11, \cdots, 20$. The test results of average MSE for Fig.2(a) and Fig.2(b) are presented in Fig.4 respectively.

According to Fig.4, it can be observed that the average reconstruction error is the lowest for $h(x) = [\sin(\frac{\pi}{2}x)]^2$ while it is the biggest for $h(x) = x^{0.5}$.

We conclude that the reconstruction performance of GOM is better than that of the traditional and fractional-order orthogonal moment by choosing appropriate $h(x)$.

$h(x)$	$x^{0.5}$	x	$x^{1.5}$	$\sin(\frac{\pi}{2}x)$	$\sin(\frac{\pi}{2}x^2)$	$[\sin(\frac{\pi}{2}x)]^2$
$n_{\max}=m_{\max}=5$						
MSE	0.3691	0.3088	0.2870	0.2583	0.2755	0.2551
$n_{\max}=m_{\max}=10$						
MSE	0.2297	0.1903	0.1862	0.1743	0.1665	0.1559
$n_{\max}=m_{\max}=15$						
MSE	0.1650	0.1449	0.1433	0.1276	0.1254	0.1076
$n_{\max}=m_{\max}=20$						
MSE	0.1381	0.1138	0.1103	0.0999	0.0957	0.0930

Fig.3 Image reconstruction using GLMs

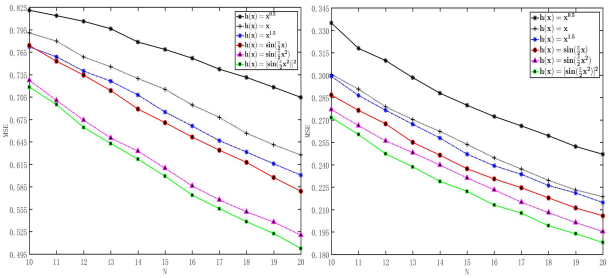

(a) (b)

Fig.4 Average reconstruction errors of 30 Chinese characters in Fig.2(a) and Coil-20 images in Fig.2(b) with different $h(x)$: (a)Results for Fig.2(a) , (b)Results for Fig.2(b).

B. *Rotation invariance*

Recognition rate is defined as follows :

$$\gamma = \frac{n_r}{N_t} \tag{19}$$

where n_r is the number of correctly classified images and N_t is the total number of test images. It is employed to test the rotation invariance in polar coordinate system.

Each image in Fig.2(a) and Fig.2(b) is rotated by angles of $15^\circ - 355^\circ$ with 20° increments. Consequently, 18 test images are obtained for every image in Fig.2(a) and Fig.2(b). Set $n_{\max} = m_{\max} = 2$, consequently, nine $\left|GLM_{nm}^{P}\right|$ are used as invariant features. The test results show that the recognition rates are all 100% when taking different $h(x)$ above by using minimum distance method for classification with regard to 30 binary images. Results for grayscale images in Fig.2(b) are similar in Fig.2(a). Thus, GLMs in polar coordinate system are rotation invariant.

C. *Robustness to noise*

In practice, images are usually degraded by noise. We rotate images in Fig.2(a), Fig.2(b) and further add different density Salt & Pepper noise and Gaussian noise to the rotated images.

1) Robustness to Salt & Pepper noise

The images in Fig.2(a) are rotated as aforementioned, and then the rotated images are added by Salt & Pepper noise with density of 0.015 , 0.030 , 0.045 , 0.060 and 0.075 respectively. The recognition rates for these tested images are shown in Fig.5(a). It is observed that the robustness to noise of GLMs is the best for $h(x)=[\sin(\frac{\pi}{2}x)]^2$.

Further, the images in Fig.2(b) are rotated, and then the rotated images are also added by Salt & Pepper noise with density of 0.05 , 0.10 , 0.15 , 0.20 and 0.25 respectively.The recognition rates for these tested images are presented in Fig.5(b). Similarly, the robustness to noise is also the best for $h(x)=[\sin(\frac{\pi}{2}x)]^2$.

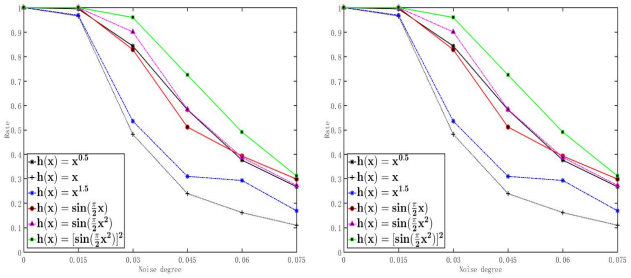

(a) (b)

Fig.5 Recognition rates of different $h(x)$ for images in Fig.2(a) and Fig.2(b) under Salt & Pepper noise: (a) Fig.2(a) (b) Fig.2(b)

Hence, the robustness to Salt & Pepper noise of GLMs is better than that of the traditional and fractional-order orthogonal moment when we choose appropriate $h(x)$.

2) Robustness to Gaussian noise

Images in Fig.2(b) are rotated as aforementioned, and then the rotated images are added by Gaussian noise with density of 0.02, 0.04, 0.06, 0.08 and 0.10 respectively. The recognition rates for these tested images are shown in Fig.6. It is observed that the robustness of GLMs to Gaussian noise is outstanding when we choose $h(x)=[\sin(\frac{\pi}{2}x)]^2$.

In conclusion, the robustness to Salt & Pepper noise and to Gaussian noise for GLMs defined in this paper are better than those for the traditional moments and fractional-order orthogonal moments.

V. CONCLUSION

Orthogonal moments offer the ability to recover the image due to their orthogonality, and are of high level noise robustness. Consequently, various orthogonal moments have been introduced. In recent years, considerable attention has been given to fractional-order orthogonal moments. However, the theoretical framework to the construction of fractional-order orthogonal moments can be further generalized.

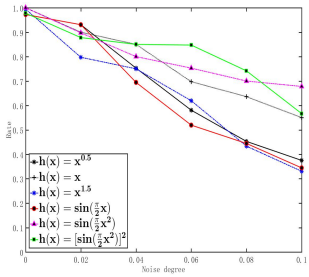

Fig.6 Recognition rate of different $h(x)$ for images in Fig.2(b) under Gaussian noise

In this paper, a general framework is set up to construct orthogonal moments, and GOMs are proposed. As an example, the GLMs are constructed with the proposed method. Orthogonality and rotation invariance of these moments are proven. Several functions have been employed to construct new set of orthogonal moments. Results show that these moments have potential for image reconstruction and are more robust to noise.

ACKNOWLEDGMENT

This work was supported in part by the National Science Foundation of China under Grant 61572015, 41375115, and 11301276.

REFERENCES

[1] Flusser J, Suk T, Zitova B. Moments and moment invariants in pattern recognition . Chichester: John Wiley & Sons, 2009:46-43.

[2] Zhu H H, Yang Y, Gui H Z,et al. Image analysis by generalized Chebyshev-Fourier and generalized pseudo-Jacobi-Fourier moments. Pattern Recognition, 2016, 51(3): 1-11.

[3] Lan R S, Zhou Y C, Tang Y Y. Quaternionic local ranking binary pattern: a local descriptor of color images. IEEE Trans. Image Process,2016, 25(2): 566-579

[4] Lan R S, Zhou Y C. Quaternion-Michelson descriptor for color image classification. IEEE Trans. Image Process. 2016, 25(11): 5281-5292 (2016)

[5] Broumandnia H A. Shanbehzadeh J. Fast Zernike wavelet moments for Farsi character recognition. Image Vision Computing, 2007, 25:717-729.

[6] Singh C. Improved quality of reconstructed images using floating point arithmetic for moment calculation. Pattern Recognition, 2006, 39: 2047-2064.

[7] Li S, Lee M C, Pun C M. Complex Zernike moments features for shape based image retrieval. IEEE Transactions on Systems, Man, and Cybernetics: Part A: Systems Humans, 2009, 39(1):227-237.

[8] Deng A W, Wei C H, Guo C Y. Stable, fast computation of high-order Zernike moments using a recursive method. Pattern Recognition, 2016, 56: 16-25.

[9] Xiao B, Li L P, Li Y, Li W S, Wang G Y. Image analysis by fractional-order orthogonal moments. Information Science,2017, 382-383: 135-149.

[10] Zhang H, Li Z, Liu Y. Fractional orthogonal Fourier-Mellin moments for pattern recognition. Chinese Conference Pattern Recognition. Springer, 2016.pp.766-778.

[11] Benouini R, Batioua I, Zenkouar K, et al. Fractional-order orthogonal Cheyshev moments and moment invariants for image representation and pattern recognition. Pattern Recognition, 2019,86:332-343.

[12] Chen B, Yu M, Su Y Q,et al. Fractional quaternion Zernike moments for robust color image copy-more forgery detection. IEEE Access 2018, 6(c),56637-56646.

[13] Xiao B, Wang G Y,Li W S. Radial shifted Legendre moments for image analysis and invariant image recognition . Image and Vision Computing, 2014, 32(12): 994-1006.

[14] Shu H Z, Luo L M, Yu W X, et al. A new fast method for computing Legendre moments. Pattern Recognition, 2000, 33(2):341-348.

[15] Sheng Y L, Shen L X. Orthogonal Fourier–Mellin moments for invariant pattern recognition. Journal of the Optical Society of America A, 1994, 11(6):1748-1757.

[16] Lan R S, He J W, Wang S H et.al, A parameter-selection-based chaotic system. IEEE Trans. Circuits Syst. II Express Briefs 2019,66-II(2): 492-496

[17] Lan R S, Zhou Y C,Liu Z B, Luo X N. Prior knowledge-based probabilistic collaborative representation for visual recognition. IEEE Trans. Cybern. 2020,50(4): 1498-1508